BMC Microbiology

RESEARCH

Open Access

# The high efficiency protective effectiveness of a newly isolated myoviruses bacteriophage vB_AceP_PAc in protecting mice from *Aeromonas caviae* infection in mice

Chao Feng[1†], Lu Wang[2†], Huifang Bai[1], Qixing Huang[1], Shuang Liang[1], Ruiqi Liang[1], Jiahao Yu[1], Shun Wang[1], Hui Guo[1], Sayed Haidar Abbas Raza[4], Xiaofeng Shan[1], Dongxing Zhang[1], Wuwen Sun[1,3*] and Lei Zhang[1,3*]

**Abstract**

Phage therapy is an effective strategy to combat multidrug resistance in bacteria and has been increasingly utilized to protect animals from bacterial infections. This study involved the isolation and purification of a novel myoviruses phage, vB_AceP_PAc, from a drug-resistant bacterial strain *Aeromonas caviae*. Genome sequence analysis based on nucleotide sequences revealed that vB_AceP_PAc shared significant similarity with the genomes of 10 other *Aeromonas* phages, with the highest coverage rate of 52% with phiA047. Intraperitoneal injection of $1\times10^7$ CFU/mL (100 µL/mouse) *A. caviae* AC-CY resulted in diarrhea in mice three days later. At this time, oral administration of $1\times10^9$ PFU/mL (100 µL/mouse) vB_AceP_PAc effectively alleviated the diarrhea induced by *Pseudomonas aeruginosa* infection in the mice. Furthermore, oral administration of $1\times10^9$ PFU/ml vB_AceP_PAc (100 µl/mouse) in healthy mice significantly reduced inflammatory cytokine levels, increased tight junction molecule levels, and improved intestinal barrier function. Moreover, the consumption of vB_AceP_PAc by health mice led to a significant increase in the abundance of *Lactobacillaceae* in the gut, while the expression of $CD3^+CD4^+/CD3^+CD8^+$ was minimally affected. Overall, the findings of this study confirmed the promising potential of bacteriophage vB_AceP_PAc in treating diarrhea caused by *A. caviae*.

**Keywords** Bacteriophage, Genome analysis, Gut microbiota, Intestinal barrier function, Diarrhoea

†Chao Feng and Lu Wang contributed equally to this work.

*Correspondence:
Wuwen Sun
sunwuwen@borui.com
Lei Zhang
zhanglei0221@jlau.edu.cn
[1]College of Animal Science and Technology, Jilin Agricultural University, Changchun 130118, China
[2]Institute of Intelligent Oncology, Chongqing University, Chongqing 400030, China
[3]Postdoctoral Scientifc Research Workstation, Changchun Borui Science and Technology Co., Ltd., Changchun 130000, China
[4]College of Animal Science and Technology, Northwest A&F University, Yangling, Shaanxi 712100, China

## Introduction

*Aeromonas caviae* is a Gram-negative, facultative anaerobic bacterium of the genus *Aeromonas*, which commonly inhabits freshwater, river water, seawater and sewage. This zoonotic pathogen has the capacity to induce various infections in humans, including those of the urinary system, respiratory tract, biliary tract and may even be lethal in certain instances [1–3]. It is also a significant pathogen for fish and other cold-blooded animals [4]. Based on a single genome analysis, *A. caviae* contains many putative virulence genes, including those encoding a type 2 secretion system, an RTX toxin, and polar flagella [5]. *A. caviae* movement requires the expression of a single polar flagellum that is crucial for adhesion to intestinal epithelial cells. The glycosylation of flagellin may help the bacteria evade recognition by the host immune system, thereby enhancing its pathogenicity [6]. Antibiotics currently represent the principal mode of treatment for *A. caviae* infections. However, the widespread use of clinical antibiotics has led to the development of multidrug resistance in *A. caviae*, including increasing resistance to carbapenem antibiotics [7, 8]. The rising incidence of drug-resistant *A. caviae* underscores the urgency to explore alternative treatment strategies.

Bacteriophages (Phages) are widely found in various habitats, such as soil, wastewater, and aquatic environments, and are typically capable of infecting bacteria [9]. Their specificity makes them a promising therapeutic option. Due to their ability to lyse their bacterial hosts, lytic phages have been applied in a wide variety of scenarios to combat bacterial pathogens, including therapy (as therapeutic and prophylactic), biocontrol, sanitation, preservation, detection, and remediation [10–15]. Lytic phages are considered the most promising candidates for therapeutic use, as they efficiently kill bacterial hosts. In contrast, temperate phages can coexist with the host, which introduces the potential risk of lysogenic conversion [16].

The safety and efficacy of bacteriophage preparations are key considerations in their application. Studies indicate that bacteriophages can modulate responses in eukaryotic immune cells, emerging as a significant approach to regulate host immunity and combat pathogenic bacteria in clinical settings [17]. It has been reported that bacteriophages can regulate both innate and adaptive immunity through processes such as phagocytosis and cytokine response [18]. Furthermore, bacteriophages can influence the immune and metabolic potential of the intestine by perturbing the stability of the intestinal microbiota [19]. In this study, we identified a novel bacteriophage, vB_AceP_PAc, which exhibited a therapeutic effect on mouse diarrhea induced by drug-resistant *A. caviae*. Our investigation focused on assessing the impact of the phage on intestinal morphology, inflammatory cell secretion, and intestinal microbiota in mice during phage administration, with the aim of establishing a foundation for the broader application of bacteriophages.

## Materials and methods

### Mice and ethics statement

Four-week-old female BALB/c mice were obtained from Beijing Vital River Laboratory Animal Technology Co., Ltd., in China, and housed in a pathogen-free environment at Jilin Agriculture University. The mice were maintained under alternating 12-hour light and 12-hour dark cycles at a temperature of 25 ± 3 °C. All animal procedures were conducted in accordance with the approval of the Animal Care and Use Committee of Jilin Agriculture University (Protocol number: JLAU202208150021), and the animal facility was fully accredited by the National Association for Laboratory Animal Care.

### Strains and phage

Multidrug-resistant *A. caviae* AC-CY, which was resistant to penicillins, cephalosporins, tetracyclines, macrolides, lincosamides, and glycopeptides, was isolated from diseased silver carp and maintained in our laboratory [20]. This strain was utilized for phage isolation in the present study. The phage vB_AceP_PAc was isolated from sewage systems in Changchun, China, with isolation, plaque assays, and spot tests conducted according to previously reported methods [21]. Specifically, 5 µl of phage ($1 \times 10^7$ PFU/mL) was spotted on plates containing different *Aeromonas* strains to assess host range. After overnight incubation, the zone of lysis of the susceptible host was observed. The study encompassed 13 strains of *Aeromonas* housed in the laboratory of Jilin Agricultural University (Two strains of *A. caviae* were isolated from diseased silver carp, five strains of *A. veronii* were isolated from diseased carp, and six strains of *A. hydrophila* were isolated from yellow catfish), and 25 strains donated by the Changchun Veterinary Research Institute, Chinese Academy of Agricultural Sciences, Changchun, China (Three strains of *A. caviae*, and twenty-two strains of *A. hydrophila*).

### Biological characteristics of the phage

The *A. caviae* AC-CY and bacteriophage vB_AceP_PAc were counted separately, then they were mixed at different multiplicities of infection (MOI) of 100, 10, 1, 0.1, 0.01, and 0.001, and incubated in liquid LB medium at 37 °C for 5–6 h. The titer of bacteriophage at each multiplicity of infection was determined using the double-layer plate method.

To estimate the latent period and burst size of the bacteriophage, we performed a one-step growth curve analysis following the method outlined by Kropinski [22], with

slight modifications. Initially, *A. caviae* AC-CY was cultured in LB medium until reaching the logarithmic phase ($OD_{600}$ = 0.6). Subsequently, the culture was infected with bacteriophage vB_AceP_PAc at a MOI of 1 and allowed to adsorb at 37 °C for 5 min. Following this, the cultures underwent centrifugation to eliminate unabsorbed bacteriophage, and the pellet was resuspended in 10 ml of LB. A portion of the culture (0.1 ml) was then transferred to 9.9 ml of LB, and this process of 10-fold serial dilution was repeated twice before incubation at 37 °C. Every 10 min, 0.1 ml samples were collected from each flask for PFU (Plaque Forming Unit) determination through plaque assay on a double-layer LB plate (The experiment was repeated three times).

To assess pH stability, the impact of different pH levels on vB_AceP_PAc ($1.0 \times 10^7$ PFU/mL) was investigated. The bacteriophage was incubated in LB broth adjusted to pH values ranging from 2 to 13 for 1 h. Subsequently, aliquots were taken to determine the phage titers at various pH levels. In thermal stability testing, 2 ml of bacteriophage ($1 \times 10^7$ PFU/mL) was subjected to temperatures of 4 °C, 25 °C, 37 °C, 50 °C, 60 °C, 70 °C, and 80 °C. At 10-minute intervals, 100 µl samples were collected. All experiments were replicated three times.

#### Electron microscopy

Phage morphology was examined using negative staining with phosphotungstic acid. A 20 µl sample of the concentrated vB_AceP_PAc suspension was applied to copper grids that had been negatively stained with 1% phosphotungstic acid (pH 7) for 30 s. Electron microscopy was carried out using a JEOL instrument (JEM-1400, Japan) operating at 80 kV.

#### Phage DNA extraction, sequencing, and annotation

*A. caviae* AC-CY was inoculated at 1% into 800 ml of LB medium and cultured with shaking at 180 rpm for 4 h at 37 °C until reaching an $OD_{600}$ of 0.6. Bacteriophage vB_AceP_PAc was then added to amplify in the culture until it became clear. The resulting lysate was centrifuged at 8000 × g for 15 min at 4 °C to remove bacterial debris. After that, phage particles were precipitated by adding 10% polyethylene glycol 8000 and 1 M NaCl, and subsequently, they were resuspended in 5 ml of 0.01 M PBS. The phage was applied to the step gradient solution by CsCl densities of 1.45, 1.5, and 1.7 g/ml and centrifugated by 120,000 × g for 3 h at 4 °C.

According to the previous method [23], the concentrated phage suspension was diluted to various concentrations. Subsequently, it was mixed with *A. caviae* AC-CY and spread on a double-layer agar plate for counting. The phages ($\geq 10^{11}$ PFU/mL) were filtered using a 0.22 µm filter. The genomic DNA of the phage was extracted using a Universal Phage Genomic DNA Extraction Kit from Knogen (Guangzhou, China). The DNA library and sequencing of the bacteriophage genome were completed by Novogene Bioinformatics Technology Co., Ltd (Beijing, China). The operation process was briefly described as followed: A total amount of 0.2 µg DNA sample was used as input material for the DNA library preparations. Sequencing library was generated using NEBNext® Ultra™ DNA Library Prep Kit for Illumina (NEB, USA, Catalog #: E7370L) following manufacturer's recommendations and index codes were added to each sample. Briefly, genomic DNA sample was fragmented by sonication to a size of 350 bp. Then DNA fragments were endpolished, A-tailed, and ligated with the full-length adapter for Illumina sequencing, followed by further PCR amplification. After PCR products were purified by AMPure XP system (Beverly, USA). Subsequently, library quality was assessed on the Agilent 5400 system(Agilent, USA) and quantified by QPCR (1.5 nM). The qualified libraries were pooled and sequenced on Illumina platforms with PE150 strategy in Novogene Bioinformatics Technology Co., Ltd (Beijing, China), according to effective library concentration and data amount required. The assembly was performed using SPAdes v.3.11.0 software [24]. The complete sequence was annotated using NCBI Blastn [25] (accessed on 20 December 2022) and GeneMark-ES (version 4.0) [26]. The genome map of phage vB_AceP_PAc was generated using the CG View Server [27] (accessed on 15 January 2023). The tRNAs were searched using tRNAscan-SE with default parameters [28]. The phage terminal large subunit is a highly conserved and evolutionarily significant protein, commonly used for phage evolutionary relationship analysis [29]. The phage tail fiber protein is the molecular basis for the specific recognition of the host by the phage and determines its host range [30]. After performing BLASTp searches with the amino acid sequences of the phage terminal large subunit (ORF57) and the tail fiber protein (ORF93) of phage vB_AceP_PAc, phage nucleotide sequences with significant similarity were selected, and Phylogenetic trees were generated using the Neighbor-Joining method and p-distance model on MEGA 7.0 [31, 32].

#### Bactericidal activity in vitro and in vivo

Experimental methods were carried out following previous experiments with modifications [33]. *A. caviae* AC-CY was inoculated in LB medium and incubated at 37 °C and 180 rpm for 4 h until the concentration reached $1 \times 10^8$ CFU/mL ($OD_{600}$ = 0.6). At this point, the bacteriophage vB_AceP_PAc was added at MOI = 1. The culture was then incubated at 37 °C for 12 h, with $OD_{600}$ measured every hour. A bacterial culture without the phage served as the control.

To determine the minimum concentration of *A. caviae* AC-CY that induced diarrhea in mice, a study was conducted using 30 mice divided into 6 groups, each containing 5 mice [34]. The mice in each group were given intraperitoneal injections of various concentrations of *A. caviae* AC-CY ($1\times10^5$, $1\times10^6$, $1\times10^7$, $1\times10^8$, and $1\times10^9$ CFU/mL, 100 µl/mouse), while the control group received an injection of 100 µl of 0.01 M PBS. Diarrhea occurrence was monitored in the mice for 7 consecutive days.

Healthy mice were divided into three groups, with all mice receiving an intraperitoneal injection of *A. caviae* AC-CY (the minimum concentration that induces diarrhea in mice). When the mice exhibited diarrhea symptoms, the PL group and PH group were administered different concentrations of vB_AceP_PAc orally (PL group: $1\times10^6$ PFU/ml, 100 µl/mouse; PH group: $1\times10^9$ PFU/ml, 100 µl/mouse), while the control group received 0.01 M PBS orally ($n=5$). Diarrhea occurrence was monitored in the mice for 7 consecutive days.

## Feeding experiment with phage

### *Growth performance*

The method was slightly modified on the foundations of previous research [35]. The health mice were randomly divided into three groups ($n=20$). The control group was fed a commercial basic diet, while the two treatment groups (PL group and PH group) received the commercial basic diet mixed with vB_AceP_PAc at concentrations of $10^5$ PFU/3 g and $10^8$ PFU/3 g, respectively. Each mouse was fed with 3 g bacteriophage feed every day for 28 days. Mice were weighed at the start and end of the feeding trial. Mean daily gain was calculated.

### *Ileal mucosal barrier function*

During the feeding period, blood and ileal mucosal fluid samples were collected from mice in each group ($n=3$ per group) on the 0th, 7th, 14th, 21st, and 28th day. After intraperitoneal injection of sodium pentobarbital (50 mg/kg body weight), all mice were sacrificed by cervical dislocation while anesthetized. Blood samples were allowed to clot at room temperature for 30 min, followed by centrifugation at 3000 × g at 4°C for 10 min to separate serum. The serum samples were then stored at -80 °C until analysis. Enzyme-Linked Immunosorbent Assay (ELISA) kits were utilized to measure the levels of D-lactate (Jingmei Biotech Co., Ltd., Beijing, China) and Diamine oxidase (DAO) (Nanjing Cheng Jian Institute of Biotechnology, Nanjing, China) in the serum. For the ileal mucosa (0.1 g), a homogenate was prepared by mixing the tissue with 0.1 ml of 0.01 M PBS. Transforming Growth Factor-alpha (TGF-α), secretory immunoglobulin A (SIgA), and intestinal trefoil factor (ITF) were quantified in the ileal mucosa using commercial ELISA kits, following the manufacturer's protocols.

The intestinal samples weighing 100 mg from each group at 0 and 28 days were pulverized using liquid nitrogen. Subsequently, total RNA was extracted at a concentration of 100 mg tissue per milliliter using TRIzol (Invitrogen, Carlsbad, CA, USA), and cDNA was synthesized employing a reverse transcription kit (Takara Bio, Shiga, Japan). Primers from the company Kumei (Changchun, China) (Supplementary Table 1) were utilized. Real-time PCR analysis was conducted on 7500 real-time PCR assay systems (Bio-Rad, Hercules, CA, USA) with a commercial SYBR Green kit (Takara Bio, Shiga, Japan). The housekeeping gene GAPDH (glyceraldehyde-3-phosphate dehydrogenase) functioned as the internal control to determine the relative expression level of the gene of interest using the $2^{-\triangle\triangle ct}$ method [36].

### *Histopathological analysis*

In the experiment of phage therapy, the mice were euthanized by intraperitoneal injection of sodium pentobarbital (50 mg/kg body weight) 3 days after being challenged with *A. caviae* AC-CY, and 2 days after the phage treatment. Then intestinal tissue samples were collected from euthanized mice for H&E staining.

In the safety experiment of bacteriophage in healthy mice, each group of experimental mice was euthanized by sodium pentobarbital (50 mg/kg body weight) on the 0 th and 28 th day, and intestinal tissue samples were obtained. Specifically, the tissues were aseptically sampled from the mid-sections of the duodenum, jejunum, and ileum. The intestines were gently washed with 0.01 M PBS buffer, fixed in 4% paraformaldehyde, and embedded in paraffin. Sections with a thickness of 4 µm were stained with hematoxylin and eosin (H&E).

### *Flow cytometry*

Methods with flow cytometry were adopted from previous study with modifications [37]. Cells were collected from the Peyer's patches (PPs), mesenteric lymph nodes (MLNs), and spleen on day 28. In the surface phenotype assay, $1\times10^6$ cells were blocked with 10 µl CD16/CD32 for 15 min at 4 °C and stained with the indicated antibody for 30 min at 4 °C in the dark. Cells were acquired on the BD FACS-Verse™ flow cytometer (BD Biosciences, San Jose, CA, USA) and the data were analyzed using the FlowJo 10.0.7 software (BD Biosciences, San Jose, CA, USA).

## Gut microbiota analysis

Genomic DNA was extracted from the feces of healthy mice fed with vB_AceP_PAc for 28 days using a QIAamp DNA Stool Mini Kit (Qiagen Inc., Valencia, CA). The bacterial 16S rRNA genes were amplified using

the following specific primer pairs (16S V3-V4, 341F (5'-CCTAYGGGRBGCASCAG-3') and 806R (5'- GGACTACNNGGGTATCTAAT – 3') [38]. The amplicons were purified using a Qiagen Gel Extraction Kit (Qiagen, Germany). The DNA library and sequencing and analysis were completed by Novogene Bioinformatics Technology Co., Ltd (Beijing, China). The operation process was briefly described as followed: Following manufacturer's recommendations, sequencing libraries were generated with NEBNext® Ultra™ IIDNA Library Prep Kit (Cat No. E7645). The library quality was evaluated on the Qubit@ 2.0 Fluorometer (Thermo Scientific) and Agilent Bioanalyzer 2100 system. Finally, the library was sequenced on an Illumina NovaSeq platform and 250 bp paired-end reads were generated.

Paired-end reads were assigned to samples based on their unique barcodes and were truncated by cutting off the barcodes and primer sequences. Paired-end reads were merged using FLASH (Version 1.2.11) [39], a very fast and accurate analysis tool designed to merge paired-end reads when at least some of the reads overlap with the reads generated from the opposite end of the same DNA fragment, and the splicing sequences were called Raw Tags. Quality filtering on the raw tags were performed using the fastp (Version 0.20.0) software to obtain high-quality Clean Tags. The Clean Tags were compared with the reference database (Silva database https://www.arbsilva.de/for16S/18S, Unite database https://unite.ut.ee/ for ITS) using Vsearch (Version 2.15.0) to detect the chimera sequences, and then the chimera sequences were removed to obtain the Effective Tags [40]. For the Effective Tags obtained previously, denoise was performed with DADA2 or deblur module in the QIIME2 software (Version QIIME2-202006) to obtain initial ASVs (Amplicon Sequence Variants) (default: DADA2), and then ASVs with abundance less than 5 were filtered out [41]. Species annotation was performed using QIIME2 software. For 16S/18S, the annotation database is Silva Database, while for ITS, it is Unite Database. In order to study phylogenetic relationship of each ASV and the differences of the dominant species among different samples (groups), multiple sequence alignment was performed using QIIME2 software. The absolute abundance of ASVs was normalized using a standard of sequence number corresponding to the sample with the least sequences. Subsequent analysis of alpha diversity and beta diversity were all performed based on the output normalized data. In order to analyze the diversity, richness and uniformity of the communities in the sample, alpha diversity was calculated from 4 indices in QIIME2, including Observed_otus, Chao1, Shannon, and Dominance. In order to evaluate the complexity of the community composition and compare the differences between samples (groups), beta diversity was calculated based on weighted and unweighted unifrac distances in QIIME2. Cluster analysis was performed with principal component analysis (PCA), which was applied to reduce the dimension of the original variables using the ade4 package and ggplot2 package in R software (Version 3.5.3). To study the significance of the differences in community structure between groups, the adonis and anosim functions in the QIIME2 software were used to do analysis. To find out the significantly different species at each taxonomic level (Phylum, Class, Order, Family, Genus, Species), the R software (Version 3.5.3) was used to do MetaStat and T-test analysis. The LEfSe software (Version 1.0) was used to do LEfSe analysis (LDA score threshold: 4) so as to find out the biomarkers. Further, to study the functions of the communities in the samples and find out the different functions of the communities in the different groups, the PICRUSt2 software (Version 2.1.2-b) was used for function annotation analysis.

### Statistical analysis

Statistical analyses were performed using SPSS 22.0 (SPSS, INC., Chicago, IL, USA) and R software (v.3.5.3). Statistical tests were 2-sided. A value of $P < 0.05$ was used for the determination of significant differences. $*P < 0.05$ indicated a significant difference in the data; $**P < 0.01$, $***P < 0.001$.

## Results

### Biological characteristics of vB_AceP_PAc

The phage vB_AceP_PAc was isolated from sewage systems in Changchun through plaque purification. After incubation for 12 h, vB_AceP_PAc formed plaques with diameters of 1.5–2 mm (Fig. 1A). TEM (Transmission Electron Microscope) images revealed that vB_AceP_PAc had a capsid diameter of 78 ± 1 nm and a tail length of 106 ± 1 nm. These morphological characteristics confirmed its classification within the myoviruses (Fig. 1B). The host range of vB_AceP_PAc was determined against 38 strains of *Aeromonas* spp. Interestingly, apart from *A. caviae* AC-CY, vB_AceP_PAc only demonstrated lytic activity against *A. hydrophila* BSK (Table 1). Additionally, the one-step growth curve showed that vB_AceP_PAc had a short latency period of approximately 30 min, with a rise period of around 50 min. In addition, the burst size of vB_AceP_PAc was approximately 5000 PFUs per infected cell on strain *A. caviae* AC-CY (Fig. 1C). Moreover, vB_AceP_PAc was stable across a pH range of 3–11 and exhibited optimal effectiveness at pH 6–8 (Fig. 1D). At different temperatures, the phage retained full activity at 4 °C, 25 °C, and 37 °C, but its activity reduced by half at 60 °C and became completely inactivated after 40 min at 70 °C (Fig. 1E). Furthermore, vB_AceP_PAc effectively self-replicated at the optimum MOI of 1 (Fig. 1F).

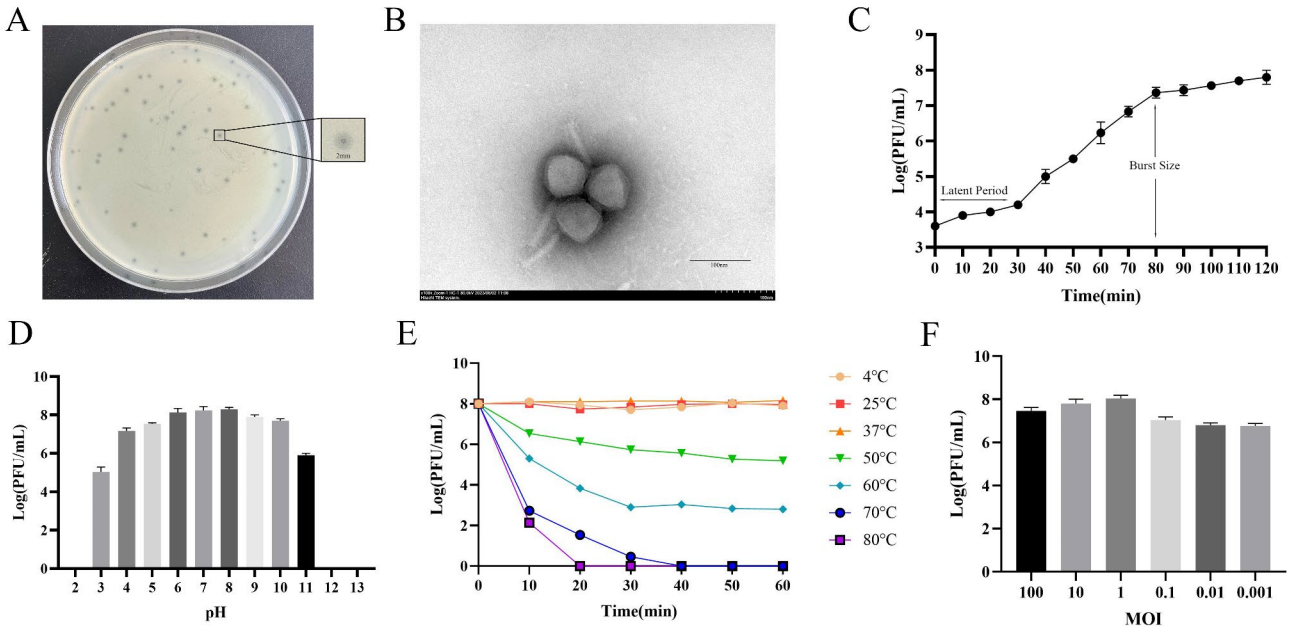


**Fig. 1** Biological characteristics of the phage vB_AceP_PAc. (**A**) phage vB_AceP_PAc lytic plaque onto *A. caviae* AC-CY culture on LB agar. Each single plaque was ≈ 2 mm in diameter. (**B**) TEM image showed the icosahedral head and sheathed tail tube with the tail fiber of vB_AceP_PAc. Bar = 100 nm. (**C**) One-step growth curve of vB_AceP_PAc. (**D**) pH stability: vB_AceP_PAc were incubated under different pH values. (**E**) Thermal stability: phage particles were incubated at different temperatures as indicated. (**F**) Determination of the MOI for vB_AceP_PAc

**Table 1** Host range of vB_AceP_PAc

| Organism | Name | vB_AceP_PAc | Organism | Name | vB_AceP_PAc |
|---|---|---|---|---|---|
| *A.caviae* | AC-CY | + | *A.hydrophila* | Ah-3-1 | - |
| *A.caviae* | ATCC15468 | - | *A.hydrophila* | Ah-NY7 | - |
| *A.caviae* | AC-6 | - | *A.hydrophila* | Ah-NY10 | - |
| *A.caviae* | AC-JY8 | - | *A.hydrophila* | Ah-23 | - |
| *A.caviae* | AC-S23 | - | *A.hydrophila* | Ah-11 | - |
| *A.veronii* | Th-0426 | - | *A.hydrophila* | Ah-57 | - |
| *A.veronii* | Av-2 | - | *A.hydrophila* | Ah-XLCJY2 | - |
| *A.veronii* | Av-3 | - | *A.hydrophila* | Ah-LHGY | - |
| *A.veronii* | Av-32 | - | *A.hydrophila* | Ah-JY1 | - |
| *A.veronii* | Av-46 | - | *A.hydrophila* | Ah-XLCJY5 | - |
| *A.hydrophila* | Ah-87 | - | *A.hydrophila* | Ah-XLCJY1 | - |
| *A.hydrophila* | Ah-138 | - | *A.hydrophila* | Ah-JY6 | - |
| *A.hydrophila* | Ah-152 | - | *A.hydrophila* | Ah-JY7 | - |
| *A.hydrophila* | Ah-BSK | + | *A.hydrophila* | Ah-XLCJY4 | - |
| *A.hydrophila* | Ah-TPS | - | *A.hydrophila* | Ah-S72-1 | - |
| *A.hydrophila* | ATCC7966 | - | *A.hydrophila* | Ah-S71-6 | - |
| *A.hydrophila* | Ah-JY22 | - | *A.hydrophila* | Ah-S71-4 | - |
| *A.hydrophila* | Ah-B3 | - | *A.hydrophila* | Ah-S57-7 | - |
| *A.hydrophila* | Ah-S60-2 | - | *A.hydrophila* | Ah-S28-6 | - |

"+" Bacteria could be cleaved by bacteriophage; "–" Bacteria could not be cleaved by bacteriophage

### Genomic characterization analysis of vB_AceP_PAc

To examine vB_AceP_PAc at the genetic level, we obtained and analyzed the complete genome sequence of vB_AceP_PAc and deposited it in GenBank (OP718284). The complete genome of vB_AceP_PAc was 123,933 bp (supplementary Table 2). The NCBI BLAST comparison at the nucleotide level indicated that only 10 bacteriophages were similar to vB_AceP_PAc, These phages had a particular phylogenetics, including *Aeromonas* phage phiA047 (OM033136.1) (percent identity: 90.31%), *Aeromonas* phage phiA009 (OM033134.1) (percent identity: 92.03%), *Aeromonas* phage phiA019 (OM033135.1) (percent identity: 92.01%), *Aeromonas* phage 2L372X (NC_048770.1) (percent identity: 85.85%),

*Aeromonas* phage 2L372D (NC_048769.1) (percent identity: 85.79%), *Aeromonas* phage 4L372D (NC_048771.1) (percent identity: 85.74%), *Aeromonas* phage vB_AdhM_TS9 (OP820701.1) (percent identity: 94.35%), *Aeromonas* phage 4L372XY (NC_048772.1) (percent identity: 86.67%), *Aeromonas* phage vB_AdhM_DL (OP820702.1) (percent identity: 90.88%), and *Pseudoaeromonas* phage VB_Pem_KLEP7 (OM654377.1) (percent identity: 76.39%). The coverage rates were all below 52%, which indicated that this phage was new at genome level (Fig. 2A). The phage genome contained 213 putative ORFs (Open Reading Frames) (Fig. 2B). After function prediction, it was shown that 29 ORFs were putatively known proteins, while 174 ORFs were unknown proteins. In addition, from the NCBI database analysis, we could not speculate on the functions of the other 10 ORFs. Genomic analysis showed that phage vB_AceP_PAc does not have integrase and other lysogenic determinants. This result indicated that the current research on functional genes of *A. caviae* phages in gene databases was limited in terms of quantity and scope. As shown in Supplementary Table 2, the proteins encoded by all ORFs ranged from 3.06 kDa to 131.39 kDa, and the smallest ORF was ORF58, which encoded 31 amino acids. The largest was ORF142, which encoded 1153 amino acids. Additional tRNA genes can expand the host range, thereby enhancing the phage's adaptability to multiple hosts, tRNAscan-SE analysis revealed that the genome of phage vB_AceP_PAc contains a single tRNA gene [42, 43]. Figure 2C shown the phylogenetic tree results based on the terminal large subunit. The results with similarity were divided into eight clades (cutoff value = 50), including *Pseudomonas* phage, *Erwinia* phage, *Acinetobacter* phage, and *Serratia* phage, *Cronobacter* phage, *Salmonella* phage, *Klebsiella* phage and a putative *Vibrio* phage. Figure 2D shown the phylogenetic tree results based on tail fiber protein, and the species selected were the same as the terminal enzyme subunit, and the phage was located in the same clades as *Aeromonas* phage 2L372X, with the closest affinity; Moreover, it was also closely related to the other two strains *Aeromonas* phage phiA047 and phiA009.

### Bacteriolytic activity of vB_AceP_PAc

To evaluate the efficacy of vB_AceP_PAc against *A. caviae* AC-CY, we conducted an in vitro time-killing assay. As depicted in Fig. 3C, the control group (PBS) exhibited a normal growth of bacteria. Conversely, in vB_AceP_PAc group, the $OD_{600}$ of *A. caviae* AC-CY decreased from 0.54 to 0.125 within 3 h of culture, but then began to growth.

Figure 3A and B illustrated the basic process of the phage therapy trial. Intraperitoneal injection of $1 \times 10^7$ CFU/mL (100 µl/mouse) of *A. caviae* AC-CY resulted in diarrhea-related symptoms, such as watery stools and fecal adherence, within three days. Therefore, $1 \times 10^7$ CFU/mL (100 µl/mouse) was established as the minimum dose of *A. caviae* AC-CY that induced diarrhea in mice (It was marked in red in Fig. 3A). When the mice exhibit diarrhea symptoms, the PL group ($1 \times 10^6$ PFU/ml, 100 µl/mouse) and the PH group ($1 \times 10^9$ PFU/ml, 100 µl/mouse) were provided with mouse feed containing varying concentrations of phages, respectively. Following continuous feeding for 2 days, the diarrhea symptoms in the PH group were significantly alleviated compared to the control group. Symptoms such as watery stools and fecal adhesion around the anal region gradually improved (Fig. 3E) (The photos were taken two days after the mice were fed with the phage-containing diet), and the intestinal villi began to recover (Fig. 3D) (Tissue samples were collected and processed for H&E staining two days after the mice were fed with the phage-containing diet).

### Effect of vB_AceP_PAc on intestinal homeostasis in mice

#### *Effect of dietary supplement of bacteriophage on the growth of mice*

Figure 4A outlines the basic process of the trial in which healthy mice were continuously fed phages for 28 days. The effects of dietary bacteriophage supplementation on mouse growth performance are outlined in Table 2. Notably, mice receiving a diet supplemented with $1 \times 10^9$ PFU/ml (100 µl/mouse) of bacteriophage vB_AceP_PAc exhibited a significant increase in final body weight ($P < 0.05$) compared to the control group. The integrity of the intestinal mucosal morphology is crucial for the mice's digestive and absorptive function. Parameters such as villus height (VH), crypt depth (CD), and the VH/CD ratio serve as direct indicators of the mucosal morphological structure and function. Our findings indicate that mice fed with a diet containing $1 \times 10^9$ PFU/ml (100 µl/mouse) of bacteriophage vB_AceP_PAc had improved VH in the duodenum, jejunum, and ileum (Fig. 4B), a reduction in CD in the duodenum (Fig. 4C), and an increased VH/CD ratio in the duodenum and ileum ($P < 0.05$) (Fig. 4D). By H&E staining, there was no obvious lesion in the intestine of mice fed with phage compared with the control group (Fig. 4E). These results suggest that the consumption of $1 \times 10^9$ PFU/ml (100 µl/mouse) vB_AceP_PAc-supplemented diets can preserve the integrity of the mouse intestinal mucosa.

#### *Dietary supplements of bacteriophage attenuated intestinal inflammation in mice*

After feeding phage vB_AceP_PAc for 28 days, the ileum mucosa of mice in the PH group showed higher levels of SIgA, ITF, and TGF-α. Notably, the PL group also increased the levels of SIgA and ITF, showed the decreasing content of TGF-α (Fig. 5A, B, C). Phage

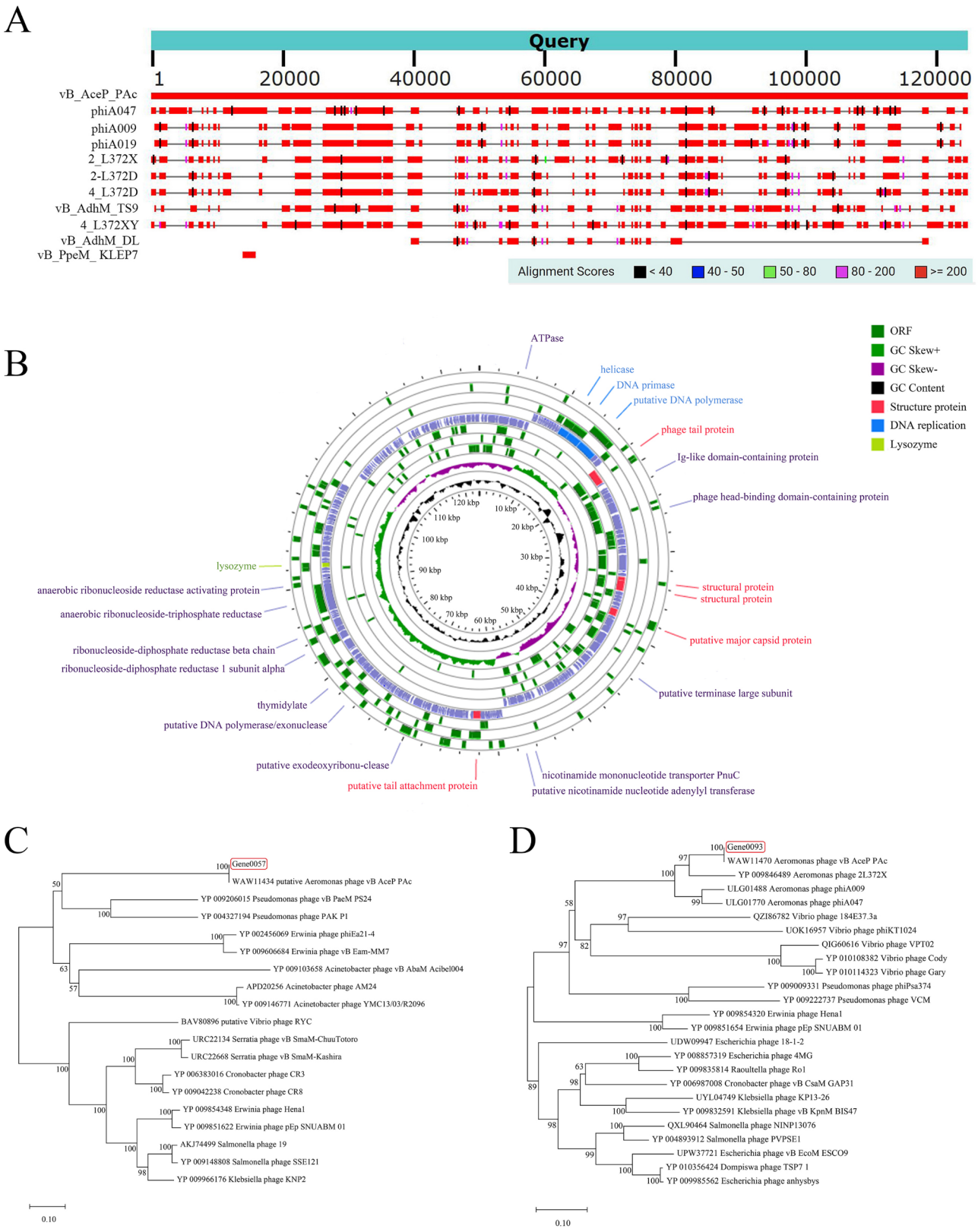


**Fig. 2** The genome characteristics of vB_AceP_PAc. (**A**) A general comparison of the genome of vB_AceP_PAc with other phages. Online plotting using NCBI BLAST (https://blast.ncbi.nlm.nih.gov/Blast.cgi). (**B**) Circular representation of vB_AceP_PAc genome. (**C**) Phylogenetic tree of the phage terminal large subunit (Numbers at each branch indicated the percentage bootstrap values on 1,000 replicates). (**D**) Phylogenetic tree of tail fiber protein

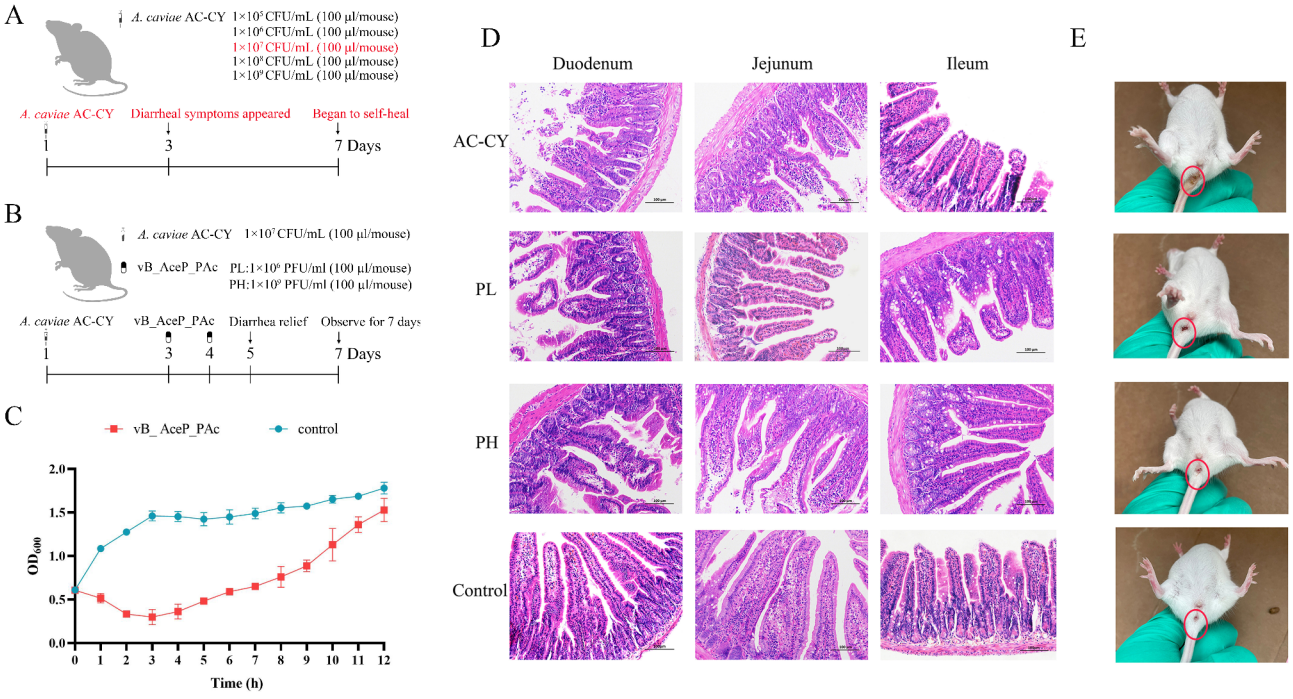


**Fig. 3** Bactericidal effect of phage against *A. caviae* AC-CY. (**A**) The dosing schedule for the minimum dose of *A. caviae* AC-CY that induces diarrhea in mice. (**B**) The administration regimen for phage therapy in mice with diarrhea. (**C**) The *A. caviae* AC-CY strain was lysed by phage vB_AceP_PAc in LB medium at 37℃. No phage was added in the negative control. The values represent the means and SD ($n=3$). (**D**) H&E staining of duodenum, jejunum, and ileum in mice with diarrhea caused by *A. caviae* AC-CY and mice in PL and PH groups. Normal mice served as the control group. (**E**) Diarrhea in mice caused by *A. caviae* AC-CY and its alleviation by feeding vB_AceP_PAc

administration significantly reduced mRNA levels of *Ccl2*, *Ccl4*, and *Icam1* in both PH and PL phage-fed groups. The administration of phages in PH group decreased mRNA levels of *IL-1β*, *IL-6*, and *TNF-α* ($P<0.01$). However, these indicators showed an increasing trend in the PL phage group ($P<0.001$) (Fig. 5D). mRNA levels of innate immune components (*Tlr2*, *Tlr4*, and *Irak4*) were also significantly up-regulated by phage administration both in PH and PL groups ($P<0.001$), however, there was no significant difference in *Tlr2* levels between the PL group and the control group (Fig. 5E). These results suggested that vB_AceP_PAc could stimulate intestinal secretion of SIgA and ITF, and down-regulated the expression of proinflammatory factors.

### *Phage improved intestinal barrier function*

Apart from the gut inflammation status, we also measured intestinal barrier function. Epithelial tight junction molecules, such as ZO-1, junctional adhesion molecule (JAM), Occludin, and Claudin 4, are the markers of epithelium integrity. Compared to the control group, dietary $1\times10^9$ PFU/ml (100 μl/mouse) bacteriophage supplementation up-regulated the relative mRNA expression of *ZO-1*, *JAM*, *Occludin*, and *Claudin 4* genes ($P<0.05$) (Fig. 6A). However, the above factors were not found to be significantly different in the PL bacteriophage diet group compared to the control group ($P>0.05$). Intestinal chemical barriers included lysozyme, Iap, Muc2, and C3gnt. qPCR results indicated that the expression of *Lysozyme*, *Muc2*, and *C3gnt* increased by feeding $1\times10^9$ PFU/ml (100 μl/mouse) bacteriophage ($P<0.001$) (Fig. 6B). The damage of the intestinal mechanical barrier led to an increase in intestinal mucosal permeability, the D-lactate and diamine oxidase (DAO) could enter the blood circulation system through the damaged intestinal mucosa, which led to the increased in serum D-lactate and DAO levels. The results of Elisa assay showed that the D-lactate concentration and DAO activity were decreased for the mice in the PH feed group ($P<0.05$). The PL fed group did reduce D- lactate concentration compared to the PH phage group (Fig. 6C, D). The results showed that feeding $1\times10^9$ PFU/ml (100 μl/mouse) vB_AceP_PAc could help maintain the integrity of the intestinal barrier.

### *Phage did not alter the CD3+CD4+/CD3+CD8+ balance in mice*

Flow cytometry was used as a mainstream tool for studying the effects of phage supplementation on immune system. Many researchers have reported that the ratio of $CD4^+/CD8^+$ cells is indicative of the general immune system status [44, 45]. Therefore, flow cytometry was performed to measure the following factors including CD3 T cells (PerCP/Cy5.5 anti-mouse CD3, clone 17A2,

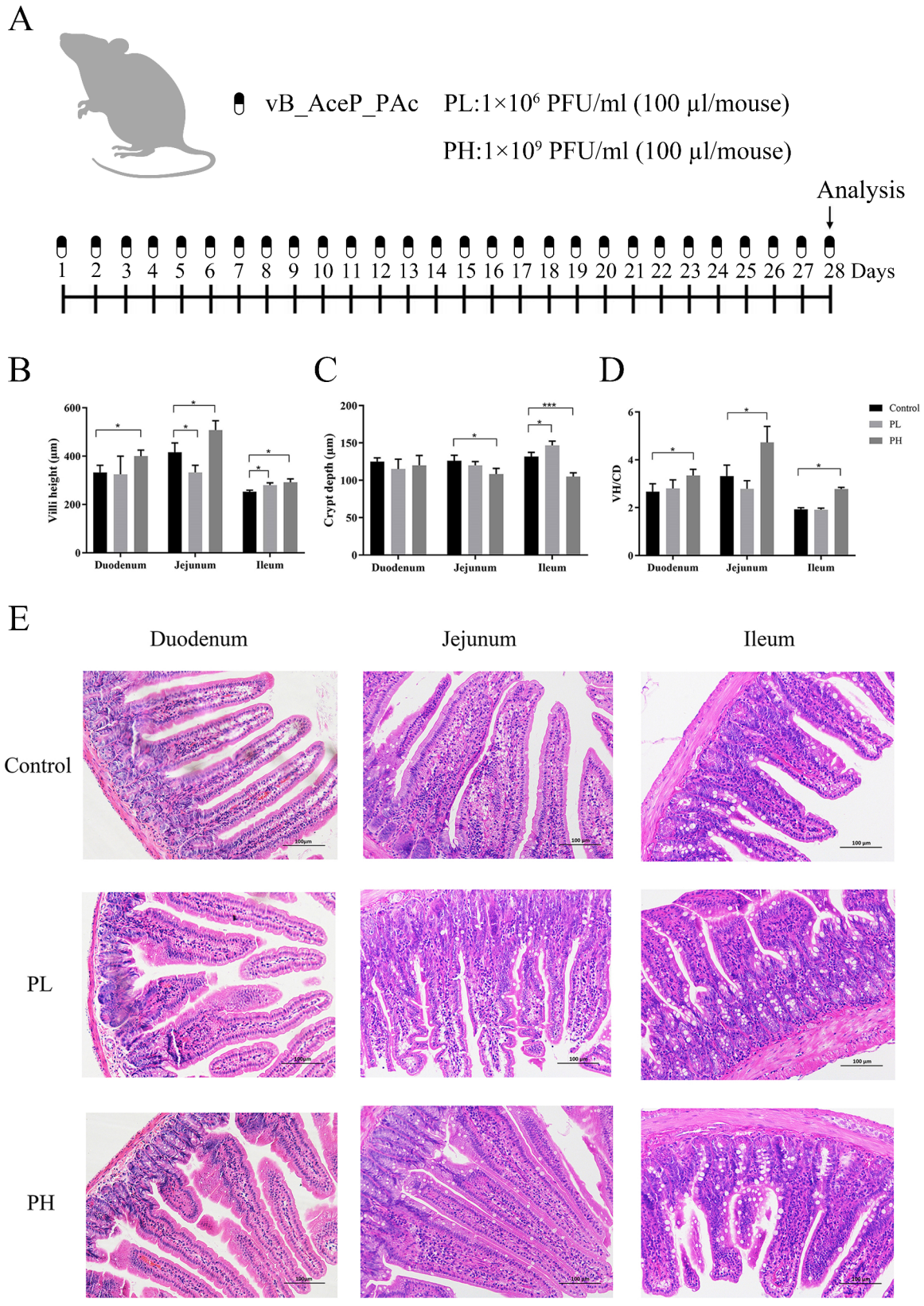


**Fig. 4** Effects dietary bacteriophage supplementation on intestinal morphology of mouse. (**A**) In the phage safety trial, healthy mice were continuously fed phages for 28 days, with sampling and analysis conducted on day 28. (**B**), Villi height; (**C**), Crypt depth; (**D**), VH/CD. The control diet was supplemented with 0.01 M PBS in the basal diet, and the treatment diets were supplemented with $10^5$ PFU/mouse and $10^8$ PFU/mouse bacteriophage in the basal diet. (**E**) The tissue samples were stained with haematoxylin and eosin

**Table 2** Effect of dietary bacteriophage supplementation on growth performance of mice ($n=3$)

| Item | Control | $10^5$ PFU/mL | $10^8$ PFU/mL |
|---|---|---|---|
| Initial body weight (g) | 17 ± 1 | 17 ± 1 | 16.6 ± 0.6 |
| Final body weight (g) | 24.6 ± 1.5 [a] | 23.3 ± 0.9 [ab] | 28 ± 1 [c] |
| Average body weight (g) | 0.271 | 0.225 | 0.407 |

a, b Different letters above bars indicates significant differences ($P<0.05$)

Biolegend, San Diego, CA, USA), CD4 T cells (CD3 CD4, FITC anti-mouse CD4, clone RM4-5, Biolegend, San Diego, CA, USA), CD8 T cells (CD3CD8, PE anti-mouse CD8a, clone 53 – 6.7, Biolegend, San Diego, CA, USA). Flow cytometry test was performed to determine the polarization of different T cell subsets in the Peyer's Patches, mesenteric lymph nodes (MLN), and spleen. Compared with the control group, feeding vB_AceP_PAc at both PL ($1\times10^6$ PFU/ml, 100 µl/mouse) and PH ($1\times10^9$ PFU/ml, 100 µl/mouse) did not change the value of $CD3^+CD4^+/CD3^+CD8^+$ in mesenteric lymph nodes (MLN), spleen, and Peyer's Patches (Fig. 7A, B, C). These results indicated that phage treatment did not affect T cell polarization in mice.

### Phage-treated mice showed different gut microbiota composition

To investigate whether phage feeding affects the gut bacteria of mice, we conducted gut microbiome sequencing. Alpha diversity is used to analyze the microbial community diversity within samples [46]. α diversity indicated that the application of bacteriophage reduced the total number of intestinal microorganisms in mice compared to the control group (Fig. 8A) and showed a higher degree of uniformity (Fig. 8B), whereas the control group had more species and higher diversity (Fig. 8C, D), which was not significantly different between the PH and PL groups (The data can be found in Supplementary

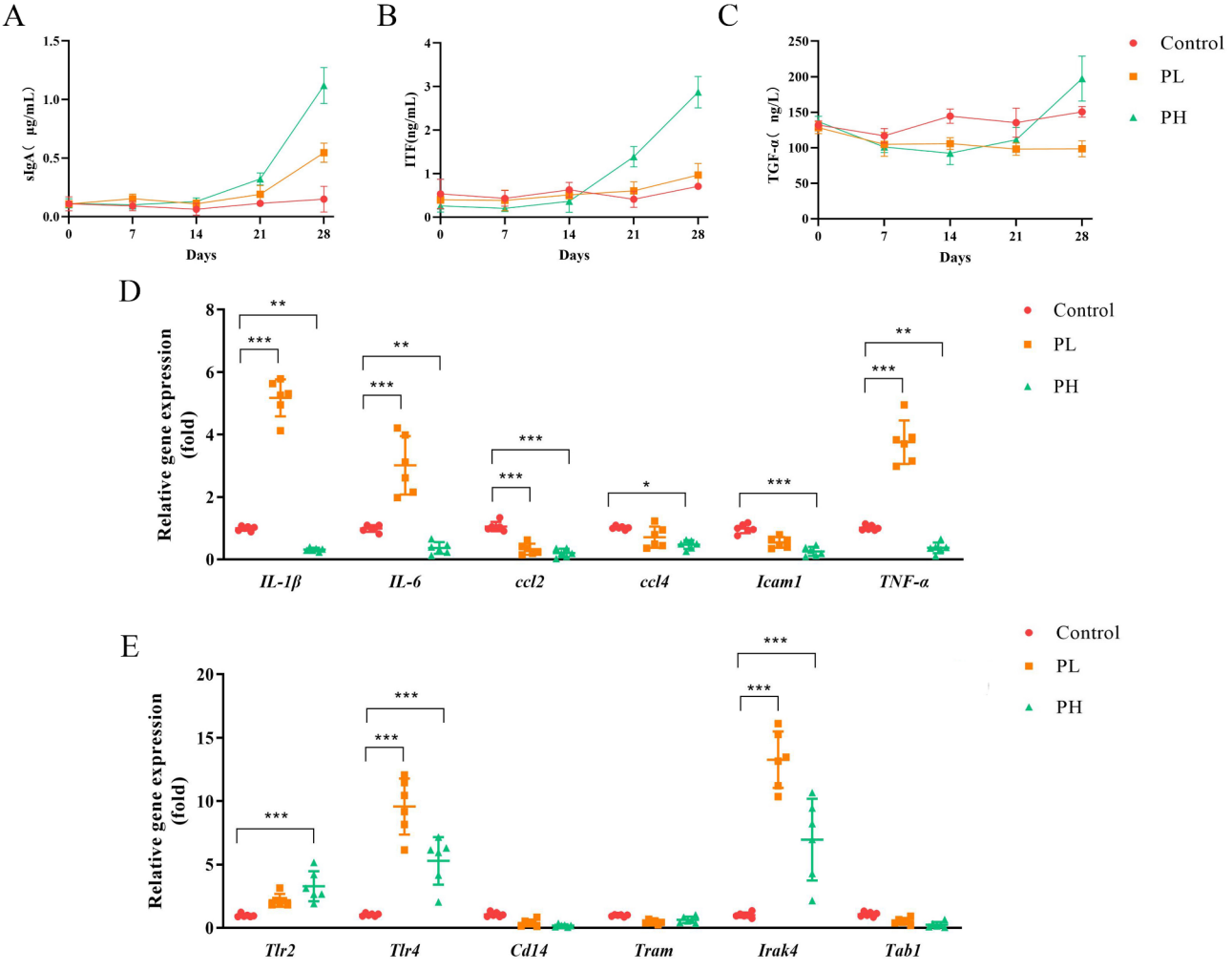


**Fig. 5** Effects of bacteriophage supplementation on intestinal inflammation in mice. (**A**) Detection of transforming growth factor-α (TGF-α), (**B**) intestinal trefoil factor (ITF), and (**C**) secretory immunoglobulin A (sIgA) in ileum mucosa of mice. (**D**) inflammatory cytokines and (**E**) innate immunity components were detected by qPCR. The data are presented as the means ± SEM

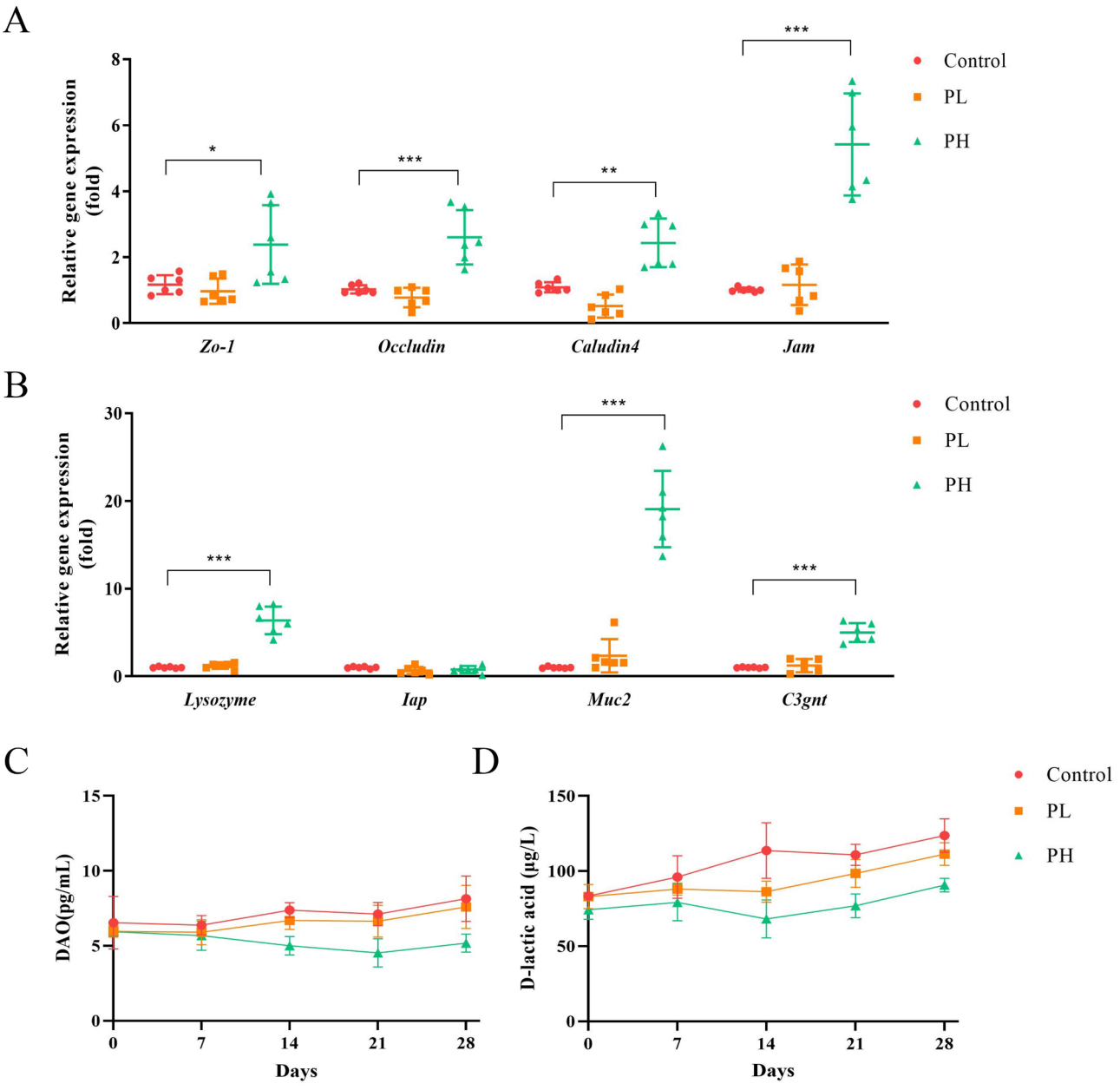


**Fig. 6** vB_AceP_PAc improved intestinal barrier function. (**A**) The mRNA levels of tight junction molecules were measured by real-time PCR. (**B**) The mRNA levels of gut mucin lysozyme, Iap, Muc2, and C3gnt in the mice of different groups were detected by qPCR. (**C**) The DAO and (**D**) D-lactate assays were performed to evaluate the Intestinal integrity of mice in the groups treated with vB_AceP_PAc

Table 3). β diversity analysis (Fig. 8E) showed significant differences between each phage group and the control group, and the analysis showed similar community composition between the PH and PL groups. Changes in the relative abundance of the microbiota shown at the phylum level and the family level are shown at Fig. 8F, and 8G respectfully. *Firmicutes* and *Bacteroidetes* were the primary phyla in caecum microbiota, followed by *Proteobacteria*. Neither PH nor PL groups phage could change the abundance of *Firmicutes*, but the phage could improve the abundance of *Bacteroidetes*. The abundance of *Proteobacteria* in the PH phage group was significantly reduced. However, the abundance of *Proteobacteria* was not affected by the PL phage group. At the family level, the abundance of *Lactobacillaceae* and *Muribaculaceae* was significantly increased, while the abundance of *Lachnospiraceae* and *Oscillospiraceae* decreased by the application of bacteriophage, with no significant difference between the two phage groups. The changes in mouse intestinal microbiota caused by PH and PL bacteriophage were mainly concentrated on the abundance of *Lactobacillus_intestinalis* in *Bacilli* and *Escherichia_Shigella* in

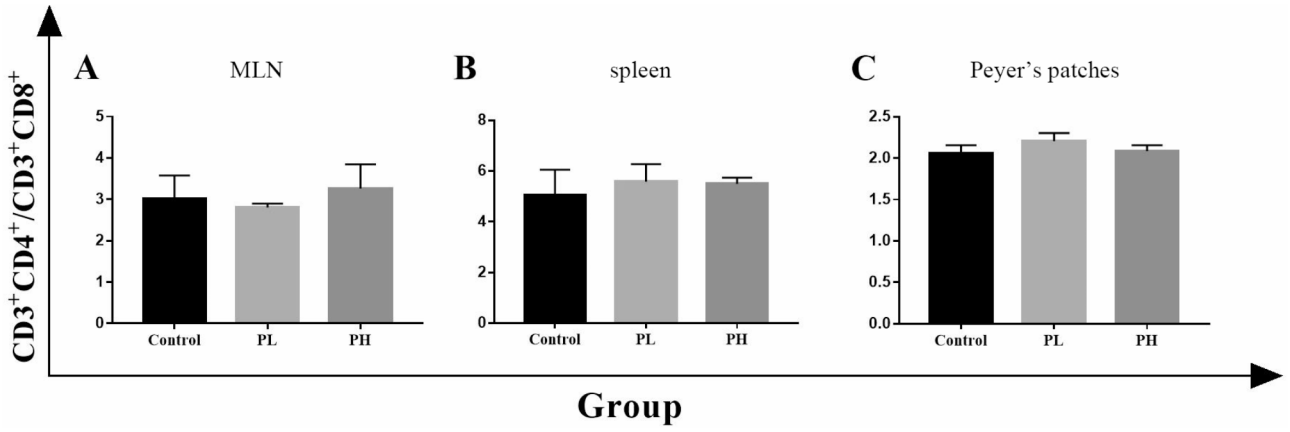


**Fig. 7** The value of $CD3^+CD4^+/CD3^+CD8^+$ in (**A**) MLN, (**B**) spleen, and (**C**) Peyer's Patches of mice fed with $1\times10^5$ PFU/mouse (PL) or $1\times10^8$ PFU/mouse (pH) phage vB_AceP_PAc

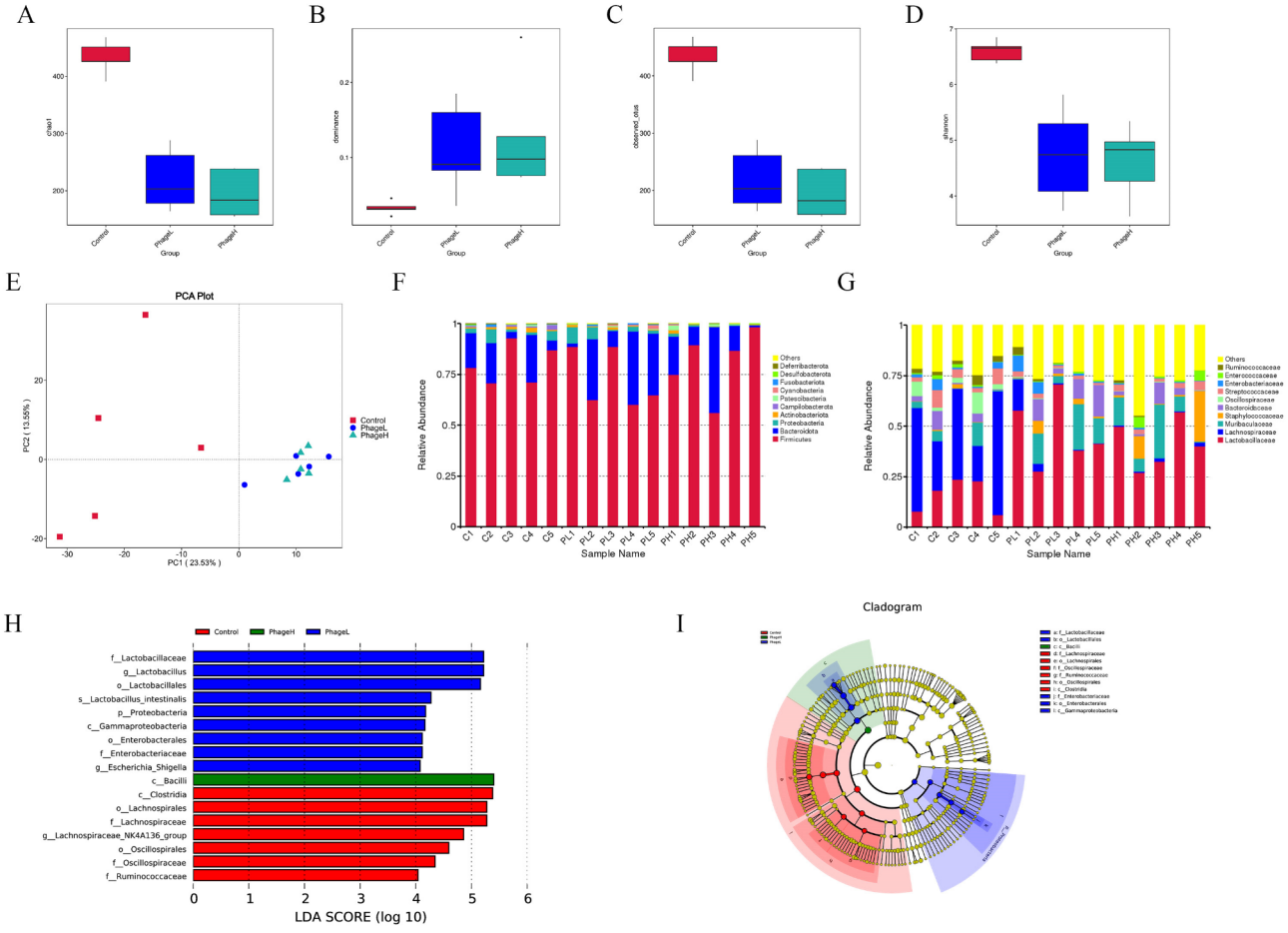


**Fig. 8** Changes of intestinal microbiota compositions of mice fed with or without dietary bacteriophage ($n=5$). α diversity changed in (**A**) chao1, (**B**) dominance, (**C**) observed otus, (**D**) Shannon. (**E**) β diversity analysis showed significant differences between each phage group and the control group. Changes in the relative abundance of the microbiota were shown at (**F**) the phylum level and (**G**) the family level. (**H**) Cladogram and LDA value distribution histogram

*Gammaproteobacteria* (Fig. 8H, I). These data indicated that the phage-treated mice had a different gut microbiota composition compared with control mice. Therefore, phage may play an important role in modulating the composition of gut microbiota.

## Discussion

In this study, we characterized a novel bacteriophage, vB_AceP_PAc. TEM confirmed that this phage exhibits morphological features typical of the myoviruses. Stability is one of the key factors for the clinical utility of bacteriophages as antimicrobial agents. Our results indicate that vB_AceP_PAc maintains the highest titer at a pH range of 6 to 8 and at temperatures below 50 °C. The complete genome of vB_AceP_PAc is 123,933 base pairs in length, closely resembling those of previously described phages, such as *Aeromonas* Phage phiA047 (GenBank accession number: OM033136.1), with which it shares 90.31% similarity, and *Aeromonas* phage phiA009 (GenBank accession number: OM033134.1), with which it shares 92.03% similarity. A BLASTp analysis of the genome identified three main gene clusters: nucleic acid metabolism and replication, host lysis, and phage structure and packaging. After a lytic phage infects the bacteria, it causes lysis of the bacterial cells and releases progeny phages [47, 48]. This process requires phage proteins with lytic functions [49]. A typical phage lysis system consists of lysin and holin proteins [50]. However, some systems may have only lysin-containing signal peptides, which can be secreted outside the membrane independently of holin [51]. The vB_AceP_PAc genome contains a single gene encoding lysozyme (ORF 148), reflecting the lysis system observed in *Aeromonas* phage phiA047 and *Aeromonas* phage phiA009. Phages that possess a higher number of tRNA genes may exhibit increased adaptability and efficiency in infecting specific hosts. This is because the presence of diverse tRNAs can enhance the translation of phage proteins within the host's cellular machinery, allowing for more effective replication and infection [42]. Conversely, phages with fewer tRNAs may be limited in their ability to infect certain hosts, potentially leading to a narrower host range [43]. The genome of vB_AceP_PAc contains only one tRNA gene, indicating a narrow host range, which was further validated in host range experiments.

The primary aim of phage therapy in clinical practice is to ensure the safe and efficient use of bacteriophages. In this study, we demonstrated that the bacteriophage vB_AceP_PAc effectively alleviated diarrhea symptoms in mice induced by infection with *A. caviae* AC-CY. Our focus has been on assessing the safety of bacteriophages in practical applications. In subsequent studies, our emphasis was on determining if the introduction of phages to the diet would elicit adverse reactions in the mice. Some studies have indicated that oral administration of bacteriophages serves as a growth promoter in pigs, increasing the average daily gain. Furthermore, oral phage therapy effectively addressed Motile *Aeromonas* Septicemia (MAS) infection in *O. niloticus* [52], and we observed similar results in mice that were fed with phages. This investigation demonstrated that dietary supplementation with $1 \times 10^9$ PFU/mL (100 µl/mouse) bacteriophage could enhance mouse growth. In order to comprehend the underlying mechanism of the growth-promoting effect of bacteriophages on mice, we collected and measured their intestinal tissues. Intestinal morphology serves as a crucial indicator of gut health and the digestive and absorptive capacity of the intestine. It is also linked to improved intestinal digestion and absorptive capacity. In this experiment, the villus height in the jejunum and ileum of mice fed with a $1 \times 10^9$ PFU/ml (100 µl/mouse) bacteriophage diet increased, confirming that the administration of $1 \times 10^9$ PFU/ml (100 µl/mouse) bacteriophage promoted the development of the intestinal tract in mice.

Bacterial toxins induce changes in membrane transport which underlie the loss of electrolyte homeostasis associated with diarrhea. A variety of virulence factors of *Aeromonas* could cause the inflammatory reactions, including heat-stable cytotonic toxins (ast), aerolysin-related cytotoxic enterotoxin (act), heat-labile cytotonic enterotoxin (alt), haemolysin (hlyA), aerolysin (aerA), type III secretion system (T3SS), elastase (ela), lipase (lip), polar flagellum (fla), and lateral flagella (laf) [53]. In *A. hydrophila*, virulence factors of aerolysin, haemolysin and multifunctional repeat-in-toxin play a vital role in the secretion of IL-1β [54]. In *A. veronii*, virulence factors of aerolysin and type III secretion system were verified to take part in the secretion of IL-1β in macrophages. In addition, *A. caviae* infection could induce the release of pro-inflammatory cytokine IL-1β [55]. The intestine could secrete bioactive substances to defend against foreign antigens, toxins, and macromolecules. It was reported that bacteriophage could be a modulator in both specific and non-specific immune response. In the present study, bacteriophage enhanced the immune capacity of mice by increasing the content of sIgA, ITF, and TGF-α in the ileal mucosa. The application of bacteriophage inhibited the expression of intestinal inflammatory factors (IL-1β, Ccl2, Icam1, and TNF-α) in mice. In line with our results, Tothova et al. [56]. reported that bacteriophage therapy decreased the expression of pro-inflammatory cytokines in mice with urinary tract infections. Similarly, Hung et al. found that bacteriophage therapy inhibited inflammatory cytokine production induced by *Klebsiella* pneumonia-mediated liver abscess and bacteremia in mice [57]. Bacteriophages were also reported to inhibit the expression of inflammatory

factors in mice. When the body was invaded by foreign pathogens, TLR2, TLR4, and other receptors were rapidly triggered [58]. The activated TLRs could provide a message about the bacterial census in the intestine, and trigger the expression of secretory anti-microbial proteins to maintain mucosal surface-related bacterial populations at homeostatic levels [59]. Our study demonstrated that the supplementation of bacteriophages in the diet enhanced the mRNA expression levels of TLR2 and TLR4 in the intestinal mucosa of healthy mice, indicating the activation of the innate immune response [60].

Proper functioning of the epithelial cells and prevention of inflammation rely heavily on the preservation of the intestinal barrier integrity, which plays a crucial role in blocking harmful bacteria from entering the body. Intestinal barrier damage increases epithelial permeability. D-lactate concentration and DAO activity were also analyzed as indicators of intestinal barrier functionality. In our experiment, the feeding with bacteriophages reduced the concentration of serum D-lactate and DAO, which indicated that the intestinal barrier function of the mice was enhanced. Tight junction proteins are the principal determinants of epithelial and endothelial paracellular barrier functions. Feeding with bacteriophages significantly improved the expression of genes associated with intestinal epithelial tight junctions, including *Zo-1*, *Jam*, *Occludin*, and *Claudin4*. In addition to tight junction molecules serving as mechanical barriers, chemical barriers, including various digestive enzymes, lysozyme, mucopolysaccharide, antimicrobial peptides, and other components secreted by the digestive tract, are also components of the intestinal mucosal barrier [61]. Lysozyme was demonstrated to bind to bacterial LPS with a high affinity to produce a complex and inhibit the biological activities of LPS [62]. Additionally, intestinal alkaline phosphatase is a gut mucosal defense factor known to dephosphorylate LPS [63]. C3GnT was responsible for the glycosylation of intestinal mucins, providing an important source of growth substrates for intestinal bacteria, which was a component of the intestinal mucosal barrier [64]. The expression levels of lysozyme (responsible for protection from bacterial infections), serving as the chemical barrier of the intestine, increased after feeding with bacteriophage. In addition, the PH group also showed up-regulation of *Muc2* and *C3gnt*. *Muc2* encodes a mucin protein that can disassociate pathogenic and commensal bacteria [65]. C3GnT is a core enzyme in the synthesis of core 3-derived *O*-glycans, the predominant components of intestinal mucus. Mice lacking glycans displayed a thinner intestinal mucus barrier [66], which represented an important source of growth substrates for intestinal bacteria [67]. Therefore, the changes in the gut chemical barrier, including those of lysozyme, *Muc2*, and *C3gnt*, influenced gut permeability.

Microbiota composition plays a crucial role in intestinal immune responses including the development of subpopulations of T lymphocytes [42]. Specifically, the $CD4^+/CD8^+$ ratio is considered a marker for an immune state that can be perturbed during inflammation and infection [68, 69]. In this study, neither the PH group nor the PL group affected $CD4^+/CD8^+$ values compared to the control group, indicating that the adaptive immune response was not activated by microbiota changes.

The gut microbiome, as a highly complex ecological system, plays a vital role in regulating the host's immune system and influences the host's development and physiological functions through the modulation of metabolic products [70–72]. The microorganisms in the gut influence the development and function of T cells through various mechanisms [73, 74]. A diverse microbiota can promote the activation and proliferation of $CD4^+$ and $CD8^+$ T cells by producing metabolites, such as short-chain fatty acids, or by interacting with intestinal epithelial cells [75]. A recent study found that phage predation not only reduced the relative abundance of target bacteria in the gut but also led to changes in untargeted bacteria through bacterial interactions, resulting in changes in certain bacteria [76]. These phage-mediated changes in the microbiome further regulated the metabolic activity of the gut microbiota [77], thereby influencing gut health [78]. In this study, the abundance of the mouse intestinal microbiota was changed and the species uniformity of the community was improved by feeding with bacteriophage, which also illustrated the regulatory effect of bacteriophage on the mouse intestinal microbiota. However, this change did not have a significant impact on the $CD4^+/CD8^+$ ratio. The increase in microbial abundance was associated with enhancing the stability of the ecosystem and resistance to pathogen invasion. By feeding bacteriophage, we found that the abundance of *Lactobacillaceae* and *Muribaculaceae* in the intestinal tract of mice was significantly increased, and the same phenomenon appeared in our previous study [79]. The present study suggested that gut microbiota regulation may be another underlying mechanism of the growth-promoting of bacteriophage for the mice.

## Conclusion

In our study, a new myoviruses phage named vB_AceP_PAc was isolated and purified from sewage using a multidrug-resistant *A. caviae*. Our results showed that vB_AceP_PAc could effectively reduce the diarrhea of mice caused by multidrug-resistant *A. caviae* AC-CY, and that the phage had certain safety in application. In addition, the application of the bacteriophage may play a role in regulating the gut microbiota of mice, which could be another potential mechanism by which the phage promoted growth in these animals.

## Supplementary Information

The online version contains supplementary material available at https://doi.org/10.1186/s12866-025-03796-w.

Supplementary Material 1

Supplementary Material 2

Supplementary Material 3

**Acknowledgements**
We thank the Changchun Veterinary Research Institute, Chinese Academy of Agricultural Sciences, Changchun, China for donating the strains used in this study.

**Author contributions**
CF, LW, HFB, QXH, SL, RQL, JHY, SW and HG performed most of the experiments. CF, SHAR, DXZ and XFS participated in the discussion. LZ and WWS supervised the work and revised the final version of the manuscript. All the authors have read and approved the final manuscript.

**Funding**
We gratefully acknowledge the financial support by the Jilin Province postdoctoral researchers funding project. Jilin Province Science and technology development plan project (No. 20220202067 N C) and (20210508006RQ).

**Data availability**
Sequence data that support the findings of this study have been deposited in the NCBI with the primary accession code OP718284.

## Declarations

**Ethics approval and consent to participate**
The animal study was reviewed and approved by the Animal Welfare and Research Ethics Committee at Jilin Agriculture University.

**Consent for publication**
Not Applicable.

**Competing interests**
The authors declare no competing interests.

Received: 16 July 2024 / Accepted: 29 January 2025
Published online: 03 March 2025

**References**

1. Pinna A, Sechi LA, Zanetti S, Usai D, Carta F. *Aeromonas caviae* keratitis associated with contact lens wear. Ophthalmology. 2004;111(2):348–51.
2. Janda JM, Abbott SL. The genus *Aeromonas*: taxonomy, pathogenicity, and infection. Clin Microbiol Rev. 2010;23(1):35–73.
3. Zhou J, Xiao T, Huang Y, Tang J, Zhang X, Jia B, Wu J. Multidrug-resistant *aeromonas caviae* causing cystitis in a renal failure patient. IDCases. 2024;37:e01999.
4. Fernández-Bravo A, Microorganisms MJFJ. An update on the Genus *Aeromonas*: Taxonomy, Epidemiology, and pathogenicity. Volume 8. Microorganisms; 2020. p. 129.
5. Sudheesh PS, Al-Ghabshi A, Al-Mazrooei N, Al-Habsi S. Comparative pathogenomics of bacteria causing infectious diseases in fish. Int J Evol Biol. 2012;2012:457264.
6. Parker JL, Lowry RC, Couto NA, Wright PC, Stafford GP, Shaw JG. Maf-dependent bacterial flagellin glycosylation occurs before chaperone binding and flagellar T3SS export. Mol Microbiol. 2014;92(2):258–72.
7. Xu S, Tu J, Zhang L, Chen Y, Dong X, Chi X, Xu H. Detection of NDM-1-Positive *Aeromonas caviae* from Bacteremia by using whole-genome sequencing. Infect Drug Resist. 2022;15:2835–41.
8. Drk S, Puljko A, Dželalija M, Udiković-Kolić N. Characterization of third generation cephalosporin- and Carbapenem-Resistant *Aeromonas* isolates from Municipal and Hospital Wastewater. Antibiot (Basel). 2023;12(3):513.
9. Wang Y, Fan H, Tong Y. Unveil the secret of the Bacteria and phage arms race. Int J Mol Sci. 2023;24:4363.
10. Martinez-Soto CE, Cucić S, Lin JT, Kirst S, Mahmoud ES, Khursigara CM, Anany H. PHIDA: A High Throughput Turbidimetric Data Analytic Tool to compare host range profiles of bacteriophages isolated using different Enrichment methods. Viruses. 2021;13(11):2120.
11. Gigante A, Atterbury RJ. Veterinary use of bacteriophage therapy in intensively-reared livestock. Virol J. 2019;16(1):155.
12. Lin DM, Koskella B, Lin HC. Phage therapy: an alternative to antibiotics in the age of multi-drug resistance. World J Gastrointest Pharmacol Ther. 2017;8(3):162–73.
13. Moye ZD, Woolston J, Sulakvelidze A. Bacteriophage applications for Food Production and Processing. Viruses. 2018;10(4):205.
14. Wei S, Chelliah R, Rubab M, Oh DH, Uddin MJ, Ahn J. Bacteriophages as potential tools for detection and control of *Salmonella* spp. Food Syst Microorganisms. 2019;7(11):570.
15. Summer NS, Summer EJ, Gill J, Young R. Phage remediation of microbe-induced corrosion; Proceedings of the 17th International Corrosion Congress: Corrosion Control in the Service of Society; Las Vegas, NV, USA. 6–10 October 2008.
16. Furfaro LL, Chang BJ, Payne MS. Applications for bacteriophage therapy during pregnancy and the Perinatal Period. Front Microbiol. 2018;8:2660.
17. Podlacha M, Gaffke L, Grabowski Ł, Mantej J, Grabski M, Pierzchalska M, Pierzynowska K, Węgrzyn G, Węgrzyn A. Bacteriophage DNA induces an interrupted immune response during phage therapy in a chicken model. Nat Commun. 2024;15(1):2274.
18. Van Belleghem JD, Dąbrowska K, Vaneechoutte M, Barr JJ, Bollyky PL. Interactions between bacteriophage, Bacteria, and the mammalian Immune System. Viruses; 2018. p. 11.
19. Górski A, Międzybrodzki R, Borysowski J, Dąbrowska K, Wierzbicki P, Ohams M, Korczak-Kowalska G, Olszowska-Zaremba N, Łusiak-Szelachowska M, Kłak M, Jończyk E, Kaniuga E, Gołaś A, Purchla S, Weber-Dąbrowska B, Letkiewicz S, Fortuna W, Szufnarowski K, Pawełczyk Z, Rogóż P, Kłosowska D. Phage as a modulator of immune responses: practical implications for phage therapy. Adv Virus Res. 2012;83:41–71.
20. Changyu L, Jiaxin T, Yang Z, Xuebin X, Aidong Q, Xiaofeng S, Yanhui L. Isolation, identification and biological characteristics of *Aeromonas caviae* from silver carp in chagan lake. Progress Veterinary Med. 2022;43:41–7. (in Chinese).
21. Hyman P. Phages for Phage Therapy: Isolation, Characterization, and Host Range Breadth. Pharmaceuticals (Basel, Switzerland).2019; 12.
22. Kropinski AM. Practical advice on the one-step growth curve. Methods in molecular biology. (Clifton N J). 2018;1681:41–7.
23. Hansen VM, Rosenquist H, Baggesen DL, Brown S, Christensen BB. Characterization of Campylobacter phages including analysis of host range by selected Campylobacter Penner serotypes. BMC Microbiol. 2007;7:90.
24. Bankevich A, Nurk S, Antipov D, Gurevich AA, Dvorkin M, Kulikov AS, Lesin VM, Nikolenko SI, Pham S, Prjibelski AD, Pyshkin AV, Sirotkin AV, Vyahhi N, Tesler G, Alekseyev MA, Pevzner PA. SPAdes: a new genome assembly algorithm and its applications to single-cell sequencing. J Comput Biol. 2012;19(5):455–77.
25. López-Moreno A, Torres-Sánchez A, Acuña I, Suárez A, Aguilera M. Representative *Bacillus* sp. AM1 from Gut Microbiota Harbor Versatile Molecular pathways for Bisphenol A Biodegradation. Int J Mol Sci. 2021;22(9):4952.
26. Sun W, Feng M, Zhu N, Leng F, Yang M, Wang Y. Genomic Characteristics and Comparative Genomics Analysis of the Endophytic Fungus *Paraphoma Chrysanthemicola* DS-84 isolated from *Codonopsis pilosula* Root. J Fungi (Basel). 2023;9(10):1022.
27. Muliya Sankappa N, Shivani Kallappa G, Kallihosuru Boregowda K, Mandrira Ramakrishna N, Kattapuni Suresh P, Shriraje Balakrishna D, Ballamoole KK, Thangavel S, Sahoo L, Lange MD, Deshotel MB, Abernathy JW. Novel lytic bacteriophage AhFM11 as an effective therapy against hypervirulent Aeromonas hydrophila. Sci Rep. 2024;14(1):16882.
28. Luo Q, Chen Z, Xu T, Huang D, Hou H, Hong C, Zhan F, Guo H, Lin Z, Guo X, Chen L, Ji ZL. Construction of integrative transcriptome to boost systematic exploration of Bougainvillea. Sci Rep. 2022;12(1):923.
29. Tsai YC, Lee YP, Lin NT, Yang HH, Teh SH, Lin LC. Therapeutic effect and antibiofilm ability assessment of a novel phage, phiPA1-3, against carbapenem-resistant Pseudomonas aeruginosa. Virus Res. 2023;335:199178.
30. Rashid MH, Revazishvili T, Dean T, Butani A, Verratti K, Bishop-Lilly KA, Sozhamannan S, Sulakvelidze A, Rajanna C. A Yersinia pestis-specific, lytic

phage preparation significantly reduces viable Y. Pestis on various hard surfaces experimentally contaminated with the bacterium. Bacteriophage. 2012;2(3):168–77.
31. Shi Z, Hong X, Li Z, Zhang M, Zhou J, Zhao Z, Qiu S, Liu G. Characterization of the novel broad-spectrum lytic phage Phage_Pae01 and its antibiofilm efficacy against *Pseudomonas aeruginosa*. Front Microbiol. 2024;15:1386830.
32. Dewanggana MN, Evangeline C, Ketty MD, Waturangi DE, Yogiara MS. Isolation, characterization, molecular analysis and application of bacteriophage DW-EC to control enterotoxigenic Escherichia coli on various foods. Sci Rep. 2022;12(1):495.
33. Kocharunchitt C, Ross T, McNeil DL. Use of bacteriophages as biocontrol agents to control *Salmonella* associated with seed sprouts. Int J Food Microbiol. 2009;128:453–9.
34. Zhang W, Zhu B, Xu J, Liu Y, Qiu E, Li Z, Li Z, He Y, Zhou H, Bai Y, Zhi F. *Bacteroides fragilis* Proagainstgantibioticbiotic-Associated Diarrhratsn Ramodulatinglating Intesdefensesfenses. Front Immunol. 2018;9:1040.
35. Zeng Y, Wang Z, Zou T, Chen J, Li G, Zheng L, Li S, You J. Bacteriophage as an alternative to antibiotics promotes growth performance by regulating intestinal inflammation, intestinal barrier function and gut microbiota in weaned piglets. Front Veterinary Sci. 2021;8:623899.
36. Livak KJ, Schmittgen TD. Analysis of relative gene expression data using real-time quantitative PCR and the 2(-Delta Delta C(T)) method. Methods (San Diego Calif). 2001;25:402–8.
37. Zhou Y, Duan L, Zeng Y, Niu L, Pu Y, Jacobs JP, Chang C, Wang J, Khalique A, Pan K, Fang J, Jing B, Zeng D, Ni X. The panda-derived *Lactobacillus plantarum* G201683 alleviates the inflammatory response in DSS-induced panda microbiota-associated mice. Front Immunol. 2021;12:747045.
38. Drengenes C, Eagan TML, Haaland I, Wiker HG, Nielsen R. Exploring protocol bias in airway microbiome studies: one versus two PCR steps and 16S rRNA gene region V3 V4 versus V4. BMC Genomics. 2021;22:3.
39. Magoč T, Salzberg SL. FLASH: fast length adjustment of short reads to improve genome assemblies. Bioinformatics. 2011;27(21):2957–63.
40. Haas BJ, Gevers D, Earl AM, Feldgarden M, Ward DV, Giannoukos G, Ciulla D, Tabbaa D, Highlander SK, Sodergren E, Methé B, DeSantis TZ, Human Microbiome Consortium, Petrosino JF, Knight R, Birren BW. Chimeric 16S rRNA sequence formation and detection in Sanger and 454-pyrosequenced PCR amplicons. Genome Res. 2011;21(3):494–504.
41. Li M, Shao D, Zhou J, Gu J, Qin J, Chen W, Wei W. Signatures within esophageal microbiota with progression of esophageal squamous cell carcinoma. Chin J Cancer Res. 2020;32(6):755–67.
42. Ali SF, Teh SH, Yang HH, Tsai YC, Chao HJ, Peng SS, Chen SC, Lin LC, Lin NT. Therapeutic potential of a Novel Lytic Phage, vB_EclM_ECLFM1, against Carbapenem-Resistant Enterobacter cloacae. Int J Mol Sci. 2024;25(2):854.
43. Liu W, Han L, Song P, Sun H, Zhang C, Zou L, Cui J, Pan Q, Ren H. Complete genome sequencing of a *Tequintavirus* bacteriophage with a broad host range against *Salmonella Abortus Equi* isolates from donkeys. Front Microbiol. 2022;13:938616.
44. Hussain T, Kulshreshtha KK, Yadav VS, Katoch K. $CD4^+$, $CD8^+$, $CD3^+$ cell counts and $CD4^+/CD8^+$ ratio among patients with mycobacterial diseases (leprosy, tuberculosis), HIV infections, and normal healthy adults: a comparative analysis of studies in different regions of India. J Immunoassay Immunochem. 2015;36:420–43.
45. Maeda N, Sekigawa I, Iida N, Matsumoto M, Hashimoto H, Hirose S. Relationship between $CD4^+/CD8^+$ T cell ratio and T cell activation in systemic lupus erythematosus. Scand J Rheumatol. 1999;28:166–70.
46. Li B, Zhang X, Guo F, Wu W, Zhang T. Characterization of tetracycline resistant bacterial community in saline activated sludge using batch stress incubation with high-throughput sequencing analysis. Water Res. 2013;47(13):4207–16.
47. Oh JH, Lin XB, Zhang S, Tollenaar SL, Özçam M, Dunphy C, Walter J, van Pijkeren JP. Prophages in *Lactobacillus reuteri* are Associated with Fitness Trade-Offs but can increase competitiveness in the gut ecosystem. Appl Environ Microbiol. 2019;86(1):e01922–19.
48. Vaitekenas A, Tai AS, Ramsay JP, Stick SM, Kicic A. *Pseudomonas aeruginosa* Resistanbacteriophagesphageitsnd Its Prevention by Strategic Therapeutic Cocktail Formulation. Antibiot (Basel). 2021;10(2):145.
49. Habibinava F, Zolfaghari MR, Zargar M, Shahrbabak SS, Soleimani M. vB-Ea-5: a lytic bacteriophage against multi-drug-resistant Enterobacter aerogenes. Iran J Microbiol. 2021;13(2):225–34.
50. Yang H, Linden SB, Wang J, Yu J, Nelson DC, Wei H. A chimeolysin with extended-spectrum streptococcal host range found by an induced lysis-based rapid screening method. Sci Rep. 2015;5:17257.
51. Dunne M, Leicht S, Krichel B, Mertens HD, Thompson A, Krijgsveld J, Svergun DI, Gómez-Torres N, Garde S, Uetrecht C, Narbad A, Mayer MJ, Meijers R. Crystal structure of the CTP1L endolysin reveals how its activity is regulated by a secondary translation product. J Biol Chem. 2016;291(10):4882–93.
52. Gordola KMC, Boctuanon FAU, Diolata RAA, Pedro MBD, Gutierrez TAD, Papa RDS, Papa DMD. Evaluation of phage Delivery systems on Induced Motile *Aeromonas* Septicemia in Oreochromis niloticus. Volume 1. PHAGE; 2020. pp. 189–97. (New Rochelle, N.Y.).
53. Zhou Y, Yu L, Nan Z, Zhang P, Kan B, Yan D, Su J. Taxonomy, virulence genes and antimicrobial resistance of *Aeromonas* isolated from extra-intestinal and intestinal infections. BMC Infect Dis. 2019;19:158.
54. Abuelsaad AS, Mohamed I, Allam G, Al-Solumani AA. Antimicrobial and immunomodulating activities of hesperidin and ellagic acid against diarrheic *Aeromonas hydrophila* in a murine model. Life Sci. 2013;93:714–22.
55. Yang Q, Zhang J, Liu F, Chen H, Zhang W, Yang H, He N, Dong J, Zhao P. *A. caviae* infection triggers IL-1β secretion through activating NLRP3 inflammasome mediated by NF-κB signaling pathway partly in a TLR2 dependent manner. Virulence. 2022;13:1486–501.
56. Tóthová L, Celec P, Bábíčková J, Gajdošová J, Al-Alami H, Kamodyova N, Drahovská H, Liptáková A, Turňa J, Hodosy J. Phage therapy of Cronobacter-induced urinary tract infection in mice. Med Sci Monitor: Int Med J Experimental Clin Res. 2011;17:Br173–178.
57. Hung CH, Kuo CF, Wang CH, Wu CM, Tsao N. Experimental phage therapy in treating Klebsiella pneumoniae-mediated liver abscesses and bacteremia in mice. Antimicrob Agents Chemother. 2011;55:1358–65.
58. Washburn RL, Hibler T, Kaur G, Dufour JM. Sertoli cell Immune Regulation: a double-edged Sword. Front Immunol. 2022;13:913502.
59. Bigorgne AE, John B, Ebrahimkhani MR, Shimizu-Albergine M, Campbell JS, Crispe IN. TLR4-Dependent secretion by hepatic stellate cells of the neutrophil-chemoattractant CXCL1 mediates liver response to Gut Microbiota. PLoS ONE. 2016;11(3):e0151063.
60. Beukema M, Faas MM, de Vos P. The effects of different dietary fiber pectin structures on the gastrointestinal immune barrier: impact via gut microbiota and direct effects on immune cells. Exp Mol Med. 2020;52(9):1364–76.
61. Wang W, Zhao J, Gui W, Sun D, Dai H, Xiao L, Chu H, Du F, Zhu Q, Schnabl B, Huang K, Yang L, Hou X. Tauroursodeoxycholic acid inhibits intestinal inflammation and barrier disruption in mice with non-alcoholic fatty liver disease. Br J Pharmacol. 2018;175:469–84.
62. Takada K, Ohno N, Yadomae T. Detoxification of lipopolysaccharide (LPS) by egg white lysozyme. FEMS Immunol Med Microbiol. 1994;9:255–63.
63. Estaki M, DeCoffe D, Gibson DL. Interplay between intestinal alkaline phosphatase, diet, gut microbes and immunity. World J Gastroenterol. 2014;20:15650–6.
64. Xia L. Core 3-derived O-glycans are essential for intestinal mucus barrier function. Methods Enzymol. 2010;479:123–41.
65. Bergstrom KS, Kissoon-Singh V, Gibson DL, Ma C, Montero M, Sham HP, Ryz N, Huang T, Velcich A, Finlay BB, Chadee K, Vallance BA. Muc2 protects against lethal infectious colitis by disassociating pathogenic and commensal bacteria from the colonic mucosa. PLoS Pathog. 2010; 6, e1000902.
66. Zarepour M, Bhullar K, Montero M, Ma C, Huang T, Velcich A, Xia L, Vallance BA. The mucin Muc2 limits Pathogen burdens and Epithelial Barrier Dysfunction during *Salmonella* enterica Serovar Typhimurium Colitis. Infect Immun. 2013;81:3672–83.
67. Fricke WF, Song Y, Wang AJ, Smith A, Grinchuk V, Mongodin E, Pei C, Ma B, Lu N, Urban JF Jr, Shea-Donohue T, Zhao A. Type 2 immunity-dependent reduction of segmented filamentous bacteria in mice infected with the helminthic parasite Nippostrongylus brasiliensis. Microbiome. 2015;3:40.
68. Monsalvo M, Vallejo A, Fontecha M, Vivancos MJ, Vizcarra P, Casado JL. CD4/CD8 ratio improvement in HIV-1-infected patients receiving dual antiretroviral treatment. Int J STD AIDS. 2019;30(7):656–62.
69. Bernal E, Martinez M, Campillo JA, Puche G, Baguena C, Tomás C, Jimeno A, Alcaraz MJ, Alcaraz A, Muñoz A, Oliver E, de la Torre A, Marín I, Cano A, Minguela A. Moderate to intense physical activity is Associated with Improved Clinical, CD4/CD8 ratio, and Immune Activation Status in HIV-Infected patients on ART. Open Forum Infect Dis. 2021;9(3):ofab654.
70. Shi N, Li N, Duan X, Niu H. Interaction between the gut microbiome and mucosal immune system. Military Med Res. 2017;4:14.
71. Zheng Y, Yue C, Zhang H, Chen H, Liu Y, Li J. Deoxycholic acid and Lithocholic Acid Alleviate Liver Injury and inflammation in mice with *Klebsiella pneumoniae*-Induced Liver Abscess and Bacteremia. J Inflamm Res. 2021;14:777–89.

72. Zhang Y, Hao J, Liu Z, Li Z, Teng L, Wang D. *InoHispidusspidus* Protects aghyperlipidemiaidemia by Inhibiting Oxidative Stress and Inflammation through Nrf2/NF-κB Signaling in High Fat Diemiced Mice. Nutrients. 2022;14(17):3477.
73. Lv Y, Ren G, Ren X. Changes of Intestinal Flora and Lymphocyte Subsets in Patients with Chronic Renal Failure. Evid Based Complement Alternat Med. 2021;2021:4288739. doi: 10.1155/2021/4288739. Retraction in: Evid Based Complement Alternat Med. 2023;2023:9898674.
74. Chen X, Shi S, Sun C, Li S. A study of the relationship between inflammatory Immune function and intestinal Flora in adolescent patients with First-Episode Depression. Actas Esp Psiquiatr. 2024;52(1):1–9.
75. Bhaskaran N, Quigley C, Paw C, Butala S, Schneider E, Pandiyan P. Role of short chain fatty acids in Controlling $T_{regs}$ and Immunopathology during Mucosal infection. Front Microbiol. 2018;9:1995.
76. Cheng M, Liang J, Zhang Y, Hu L, Gong P, Cai R, Zhang L, Zhang H, Ge J, Ji Y, Guo Z, Feng X, Sun C, Yang Y, Lei L, Han W, Gu J. The bacteriophage EF-P29 efficiently protects against Lethal Vancomycin-resistant *Enterococcus faecalis* and alleviates gut Microbiota Imbalance in a murine bacteremia model. Front Microbiol. 2017;8:837.
77. Belizário JE, Faintuch J. Microbiome and Gut Dysbiosis. Experientia Suppl. 2018;109:459–76.
78. Zhao H, Li Y, Lv P, Huang J, Tai R, Jin X, Wang J, Wang X. Salmonella phages affect the Intestinal Barrier in Chicks by altering the composition of early Intestinal Flora: Association with Time of Phage Use. Front Microbiol. 2022;13:947640.
79. Feng C, Jia KX, Chi T, Chen SM, Yu HB, Zhang L, Haidar ARS, Alshammari AM, Liang S, Zhu ZS, Li TX, Qi YL, Shan XF, Qian AD, Zhang DX, Zhang L, Sun WW. Lytic bacteriophage PZL-Ah152 as Biocontrol Measures against Lethal *Aeromonas hydrophila* without distorting gut microbiota. Front Microbiol. 2022;13:898961.

## Publisher's note